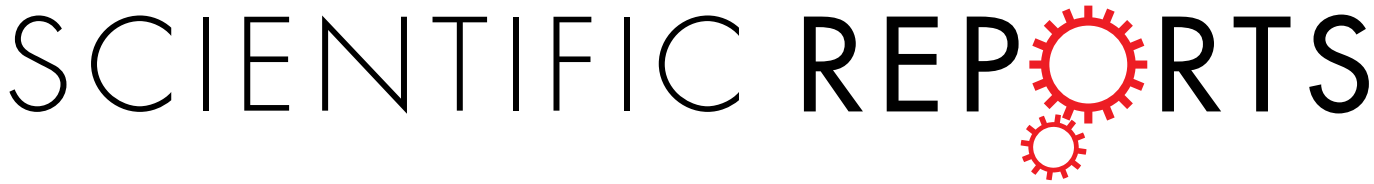

OPEN

Identification of Synergistic, Clinically Achievable, Combination Therapies for Osteosarcoma

Received: 27 May 2015
Accepted: 22 October 2015
Published: 25 November 2015

Diana Yu[1,2], Elliot Kahen[1,2], Christopher L. Cubitt[2], Jeremy McGuire[4], Jenny Kreahling[4], Jae Lee[4,6], Soner Altiok[4,7], Conor C. Lynch[4,8], Daniel M. Sullivan[2,4,9] & Damon R. Reed[1,3,4,5]

Systemic therapy has improved osteosarcoma event-free and overall survival, but 30–50% of patients originally diagnosed will have progressive or recurrent disease, which is difficult to cure. Osteosarcoma has a complex karyotype, with loss of p53 in the vast majority of cases and an absence of recurrent, targetable pathways. In this study, we explored 54 agents that are clinically approved for other oncologic indications, agents in active clinical development, and others with promising preclinical data in osteosarcoma at clinically achievable concentrations in 5 osteosarcoma cell lines. We found significant single-agent activity of multiple agents and tested 10 drugs in all permutations of two-drug combinations to define synergistic combinations by Chou and Talalay analysis. We then evaluated order of addition to choose the combinations that may be best to translate to the clinic. We conclude that the repurposing of chemotherapeutics in osteosarcoma by using an *in vitro* system may define novel drug combinations with significant *in vivo* activity. In particular, combinations of proteasome inhibitors with histone deacetylase inhibitors and ixabepilone and MK1775 demonstrated excellent activity in our assays.

Over the past few decades, there has been little progress in terms of developing more effective chemotherapies for osteosarcoma. This is true despite diligent efforts to explore many agents through collaborative trials that have included agents such as trastuzumab, interferon alfa-2b, ifosfamide, etoposide, zoledronic acid, and MTP-PE[1–5]. Current "standard of care" pediatric osteosarcoma therapy consists of three agents: high-dose methotrexate, doxorubicin, and cisplatin, with the former two being FDA-approved for this indication. Data suggest that this combination is the most effective for young adults as well, but 10-year event-free survival rates for this population are 5–10% lower than the roughly 65% pediatric rate[6–8]. Older patients are typically treated with these same agents or given a combination of doxorubicin and cisplatin, with occasional use of ifosfamide[9]. Due to osteosarcoma's rarity, clinical trials are difficult and time consuming to conduct, increasing the need for strong preclinical data to inform clinical trials. Meanwhile, many agents have been FDA-approved for adult carcinomas that cannot all be evaluated clinically for use in osteosarcoma[10].

[1]Sunshine Lab, H. Lee Moffitt Cancer Center and Research Institute, Tampa, FL 33612 Florida USA. [2]Translational Research Lab, H. Lee Moffitt Cancer Center and Research Institute, Tampa, FL 33612 Florida USA. [3]Sarcoma Department, H. Lee Moffitt Cancer Center and Research Institute, Tampa, FL 33612 Florida USA. [4]Chemical Biology and Molecular Medicine Program, H. Lee Moffitt Cancer Center and Research Institute, Tampa, FL 33612 Florida USA. [5]Adolescent and Young Adult Program, H. Lee Moffitt Cancer Center and Research Institute, Tampa, FL 33612 Florida USA. [6]Department of Biostatistics and Bioinformatics, H. Lee Moffitt Cancer Center and Research Institute, Tampa, FL 33612 Florida USA. [7]Department of Anatomic Pathology, H. Lee Moffitt Cancer Center and Research Institute, Tampa, FL 33612 Florida USA. [8]Department of Tumor Biology, H. Lee Moffitt Cancer Center and Research Institute, Tampa, FL 33612 Florida USA. [9]Department of Blood and Marrow Transplantation, H. Lee Moffitt Cancer Center and Research Institute, Tampa, FL 33612 Florida USA. Correspondence and requests for materials should be addressed to D.R.R. (email: Damon.Reed@moffitt.org)

There have been numerous preclinical efforts to better understand the pathophysiology of osteosarcoma and test agents with diverse mechanisms of actions on osteosarcoma models in order to inform future trials, including some of our own work with cell cycle inhibitors[11–15]. Furthermore, osteosarcoma occurs spontaneously in many animal species including canines where the biology, therapy and response are similar to humans[16–18]. Notwithstanding these efforts, there is not an obvious agent with sufficient activity to explore prospectively in frontline clinical trials at this time[19,20]. Sequencing of osteosarcoma tumors has demonstrated that osteosarcoma biology seems to rely on dysfunctional p53 in virtually all clinical cases with frequent translocations in intron 1 of the TP53 gene[21]. This genomic analysis revealed significant tumor-to-tumor variability through varied and numerous structural variations. As a result, a consistent therapeutic target has proven to be elusive. Despite tumor variability, we hypothesize that p53 plays a significant role in osteosarcoma tumorigenesis. For this study, we selected well-characterized cell lines that demonstrate p53 inactivation as our models. Both SAOS-2 and MG-63 have disruptions in intron 1 of TP53[22]. HOS and 143B cells are derived from the same patient and share an inactivating TP53 point mutation at position (R156P)[23]. U2OS is TP53 wildtype but contains an amplification of MDM2 rendering p53 hypofunctional[24].

We set out to develop a system to evaluate combinations of many agents that can then be rapidly translated into clinical trials in a clinically relevant manner. The methodology was optimized to incorporate past lessons learned from *in vitro* experiments that did not translate well into clinic. This was at least in part due to studied drug concentrations that were not achievable or lengths of exposure not possible as a result of metabolism[25,26]. By using largely FDA-approved agents, agents studied in pediatric trials[27], and agents with strong preliminary data for an osteosarcoma subtype, we anticipated that we could efficiently develop strong preclinical data to help inform clinical trials in osteosarcoma. All steps and experiments for combination therapy were developed and conducted in the context of the eventual clinical trial. This included careful exploration of current and previously evaluated clinical schedules that have been tolerable, demonstrated non-overlapping toxicities, included pharmacokinetic data and cytochrome P450 metabolism, and described other metabolic details that would avoid obvious drug-drug interactions.

Results

Single-agent activity at clinically achievable levels and durations. We first characterized the single-agent activity of a panel of 54 therapeutic candidates (Supplemental Table S1) using 5 pediatric osteosarcoma cell lines (143B, MNNG/HOS, MG63, U2OS, Saos2). Single-agent anti-tumor activities were assessed at C_{max}, 20% C_{max}, and 4% C_{max} using Caspase-Glo and CellTiter-Glo luminescence assays at 24 and 72 hours to indicate cell metabolism and apoptosis, respectively. Our screening results using the two assays provided collaborating evidence to indicate the most efficacious agents for the osteosarcoma cells at the tested concentrations (Fig. 1a,b). Interestingly, we obtained low Caspase-Glo signal for GSK923295A at the highest tested concentration but not at the lower concentrations. We hypothesized that the high level of GSK923295A induced a fast onset of apoptosis that could not be detected by Caspase-Glo at 24 hours due to degradation of the caspase enzyme. To verify this, immunohistochemistry was performed on osteosarcoma cells after 6-hour treatment with GSK923295A. We confirmed cell apoptosis due to the drug by demonstrating an up-regulation of caspase-3 activity relative to the vehicle controls (Fig. 1c).

Six agents that achieved >80% anti-tumor activity by CellTiter-Glo assay and >1.5-fold increase in caspase-3/7 activation were selected to move forward to combinatorial screening for potential synergistic effects (Fig. 1d). Additionally, gemcitabine, panobinostat, MK1775, and ixebepilone were selected based on promising activity as well as to expand the diversity of mechanisms of action for combinatorial testing.

Evaluation for active and synergistic combinations. We used a 5×5 checker-board matrix format that assessed each of the 10 active agents at 5 clinically achievable concentrations and multiple drug ratios to identify synergy (Supplemental Figure S1A). Full dose-response curves were obtained for the top 10 drug panel, and the CI values for all 45 combinations were calculated using CalcuSyn 2.0 and custom-designed analysis package based on the Chou and Talalay method (Supplemental Figure S1C). FA and CI values of all combinations that yielded FA > 0.85 in all 5 osteosarcoma cell lines are summarized in Supplemental Table S2. Our combination screening identified several promising drug combinations for the treatment of pediatric osteosarcoma, which were sorted by cluster analysis (Fig. 2a). Of these, we narrowed the results to 6 top combinations that produced >90% anti-tumor activity (Fig. 2b) while demonstrating strong synergy: carfilzomib:panobinostat, carfilzomib:romidepsin, bortezomib:panobinostat, bortezomib:romidepsin, MK1775:ixabepilone, and MK1775:romidpesin (Fig. 2c). Due to the steep sigmoidal drug-response curve observed for bortezomib, it was assessed at 5 concentrations with a dilution factor of 1:1.35, whereas romidepsin and panobinostat were assessed at five concentrations with a dilution of 1:2. Potentiation in bortezomib combinations was determined by fitting the dose-response relationships of single agents and drug combinations to a sigmoidal four-parameter logistic curve on a semi-log plot (Fig. 2d). Addition of 14 ng/mL panobinostat potentiated the cytotoxic effects of bortezomib by shifting the IC50 of bortezomib ~1.7-fold, from 7.45 to 4.35 ng/mL, whereas addition of 6.59 and 12 ng/mL bortezomib potentiated the cytotoxic effects of panobinostat by shifting the IC50 of panobinostat ~4.4-fold and ~4.8-fold, from 11.85 to 2.7 ng/mL and 2.5 ng/mL, respectively. Similarly, the addition of 50 and 200 ng/mL romidepsin potentiated the cytotoxicity of bortezomib by ~1.6-fold and ~2.5-fold,

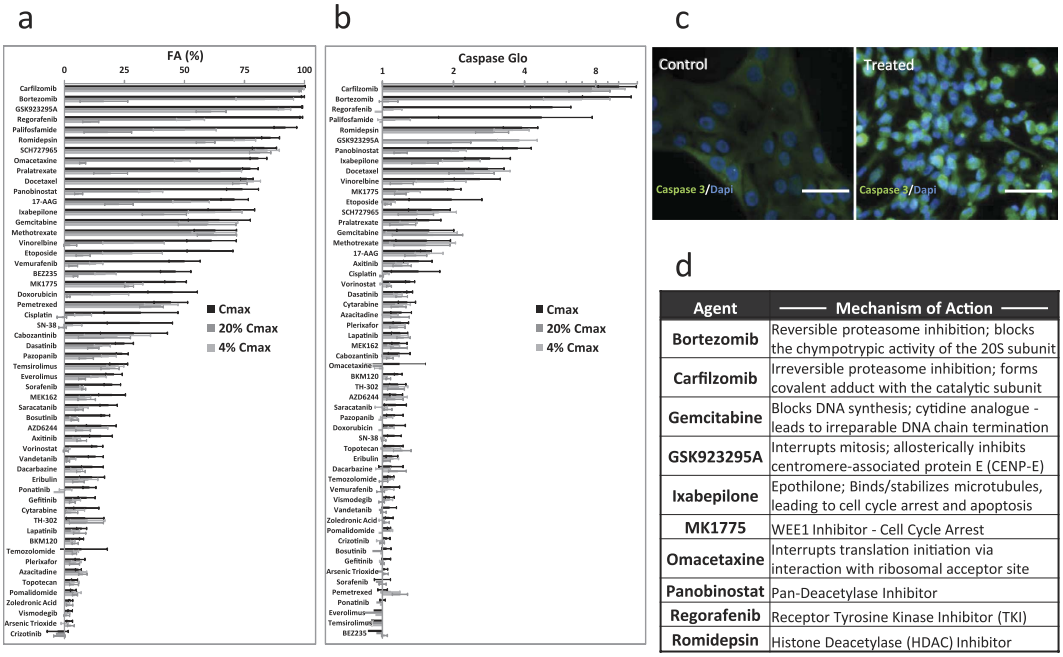

Agent	Mechanism of Action
Bortezomib	Reversible proteasome inhibition; blocks the chympotrypic activity of the 20S subunit
Carfilzomib	Irreversible proteasome inhibition; forms covalent adduct with the catalytic subunit
Gemcitabine	Blocks DNA synthesis; cytidine analogue - leads to irreparable DNA chain termination
GSK923295A	Interrupts mitosis; allosterically inhibits centromere-associated protein E (CENP-E)
Ixabepilone	Epothilone; Binds/stabilizes microtubules, leading to cell cycle arrest and apoptosis
MK1775	WEE1 Inhibitor - Cell Cycle Arrest
Omacetaxine	Interrupts translation initiation via interaction with ribosomal acceptor site
Panobinostat	Pan-Deacetylase Inhibitor
Regorafenib	Receptor Tyrosine Kinase Inhibitor (TKI)
Romidepsin	Histone Deacetylase (HDAC) Inhibitor

Figure 1. Single-agent activities of 54 therapeutic compounds screened against 5 osteosarcoma cell lines. (**a**) Percent reduction in CellTiter-Glo signal indicating decreased ATP production at 72 hours post-drug treatment (normalized to vehicle controls). (**b**) Relative fold change in Caspase-Glo signal indicating cell death 24 hours post-drug treatment (normalized to vehicle controls). (**c**) Immunocytochemistry staining of caspase-3 activity in MG63 cells after 6-hour treatment with GSK923295A (7122 ng/mL) showing caspase-3 up-regulation in response to drug treatment. (**d**) Top 10 drug candidates with diverse mechanisms-of-action were selected from single-agent screening results to be further evaluated in 45 drug combinations for synergistic effects against pediatric osteosarcoma. N = 3 biological replicates. Scale bar: 20 μm.

respectively, whereas addition of 6.59 and 12 ng/mL bortezomib potentiated the effects of romidepsin by ~4.1-fold and 6.8-fold, respectively (Fig. 2d, Supplemental Table S4). Isobologram representations for carfilzomib:panobinostat, carfilzomib:romidepsin, MK1775:ixabepilone, and MK1775:romidepsin combinations at constant drug molar ratios further demonstrated the synergistic effects of combining these agents in clinically achievable dose ranges (Fig. 2e). Moreover, we utilized the Mixlow method of synergy calculation on data points at constant molar ratios for these 4 combinations to further verify that synergy is observed at high FA levels (Supplemental Figure S2). We consistently observed strong activity and synergistic effects when combining the HDAC inhibitors romidepsin and panobinostat with the proteasome inhibitors bortezomib and carfilzomib or the cell cycle inhibitor MK1775 (Fig. 2a). In addition, we observed promising synergy between MK1775 and ixabepilone, a microtubule inhibitor.

Order-of-addition analysis of combinations of interest. To determine whether the combinatorial effects were dependent on treatment order, we next evaluated the order of addition in these 6 efficacious two-drug combinations using the 5 × 5 checker-board matrix format at 5 clinically achievable concentrations (Fig. 3a,b). A comparison of different orders of drug application and concurrent drug application showed slight variations in the FA and CI values between the osteosarcoma cell lines; however, the combinations continued to demonstrate synergy with high FA (Table 1, Supplemental Table S5). At the highest tested concentrations, bortezomib and romidepsin demonstrated similar FA levels; however, concurrent application and treatment with romidepsin 24 hours prior to bortezomib produced slightly lower CI, suggesting better synergy (Table 1, Fig. 3a,b). This is further demonstrated at additional drug ratios where treatment with bortezomib prior to romidepsin resulted in a right shift in the drug-response curve (Fig. 3d) and significant increase in the IC50 (Fig. 3f). A similar trend was observed for bortezomib and panobinostat at the highest tested levels, where concurrent application and treatment with the HDAC inhibitor prior to bortezomib produced slightly better synergy (Table 1). Drug-response plots of additional concentration ratios showed a left shift when panobinostat was given prior to bortezomib (Fig. 3d) and a decrease in the IC50 (Fig. 3f). Nevertheless, since potentiation was only observed when bortezomib followed panobinostat, but not when panobinostat followed bortezomib, the differences between the orders of addition in this case may be nominal. Interestingly, for panobinostat and carfilzomib, a proteasome inhibitor similar to bortezomib, the best synergy was achieved with concurrent application of the 2 drugs, at both the highest tested levels (Table 1) and for the drug ratio 30:14 (carfilzomib:panobinostat) (Fig. 3f), with a significantly lower CI value (Fig. 3c). Moreover, we found a pattern for carfilzomib and

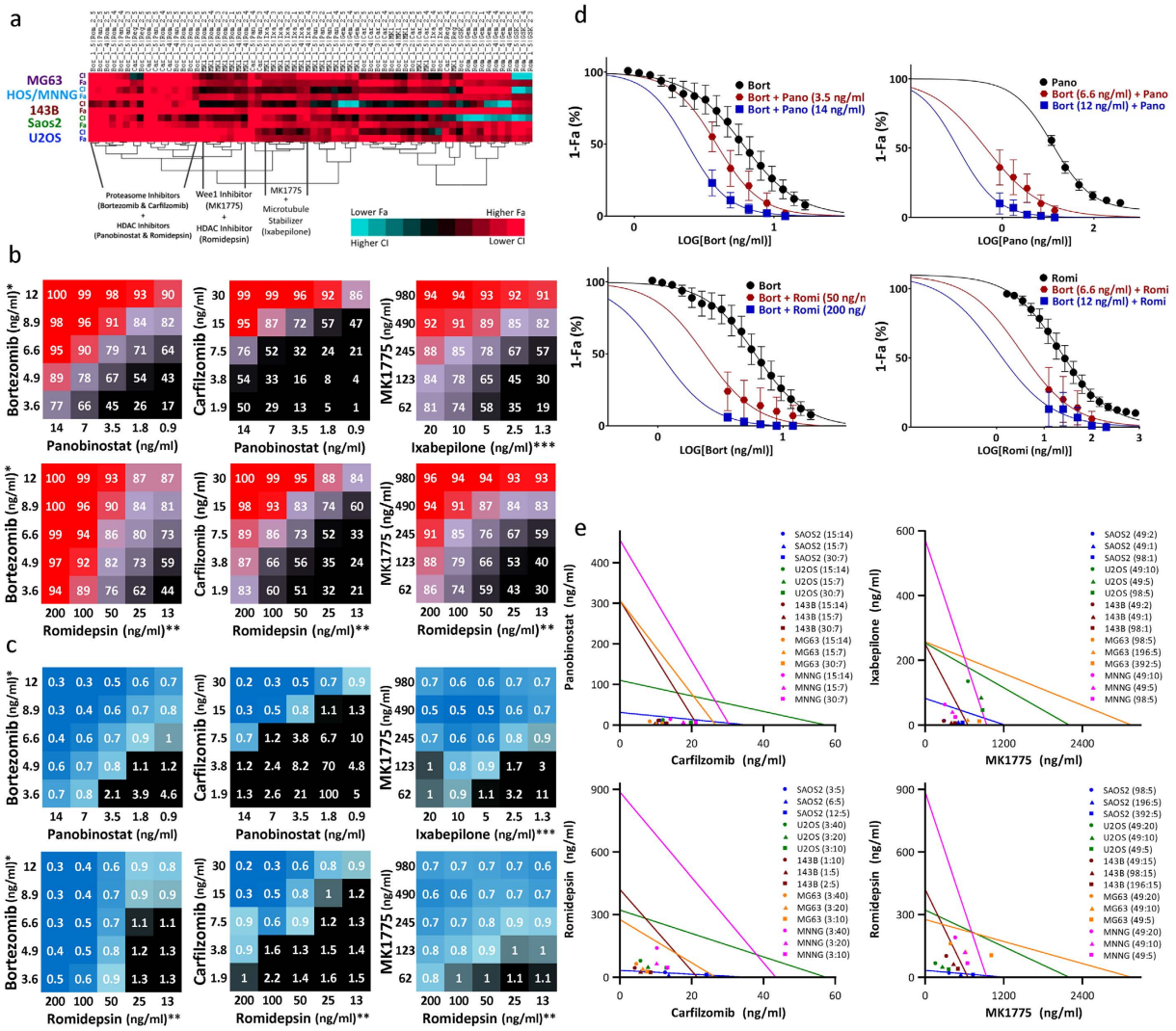

Figure 2. Combination screening results. (**a**) clustering results showing top combination picks based on FA. (**b**) FA of the top 6 combinations evaluated in 5 osteosarcoma cell lines using CT-Glo viability assay. (**c**) CI of the top 6 combinations evaluated in 5 osteosarcoma cell lines using non-constant ratio CI method. (**d**) single and combination drug-response curves for bortezomib+panobinostat and bortezomib + romidepsin combinations. (**e**), isobologram analysis of carfilzomib + panobinostat, carfilzomib + romidepsin, MK1775 + ixabepilone, and MK1775 + romidepsin at ED90. *Alternative bortezomib concentrations used with MG63 (5.00, 3.70, 2.74, 2.03, 1.50 ng/mL). **Alternative romidepsin concentrations used with 143B (150, 75.0, 37.5, 18.8, 9.40 ng/mL); Saos2 (25.0, 12.5, 6.25, 3.13, 1.56 ng/mL). ***Alternative ixabepilone concentrations used with U2OS; MNNG/HOS (100, 50.0, 25.0, 12.5, 6.25 ng/mL); MG63 (25.0, 12.5, 6.25, 3.13, 1.56 ng/mL). The exact drug concentrations used are summarized in Supplemental Table S3.

romidepsin similar to that of bortezomib and romidepsin (Fig. 3c,e), indicating that the 2 proteasome inhibitors may elicit similar intracellular events when combined with Romidepsin, and we noted that the presence of romidepsin, either concurrently or prior to proteasome inhibition, may be important for enhanced synergy. In contrast to the preferred order of addition of romidepsin prior to or concurrent with the proteosome inhibitors, we found a trend of reduced efficacy and synergy when romidepsin was applied before MK1775 (Table 1, Fig. 3c,e). Finally, varying the order of addition of MK1775 and ixabepilone demonstrated slight improvement in synergy when ixabepilone was applied before MK1775 (Fig. 3c,e).

Cytotoxicity of combinations of interest in an *ex vivo* xenograft and in normal cells. These top 6 combinations were also studied in an ex-vivo assay from a murine xenograft derived from a 50-year-old patient who had unresectable, metastatic osteosarcoma at diagnosis that progressed through multi-agent chemotherapy. Excellent efficacy was seen in 5 of the 6 combinations, and synergy was observed for all

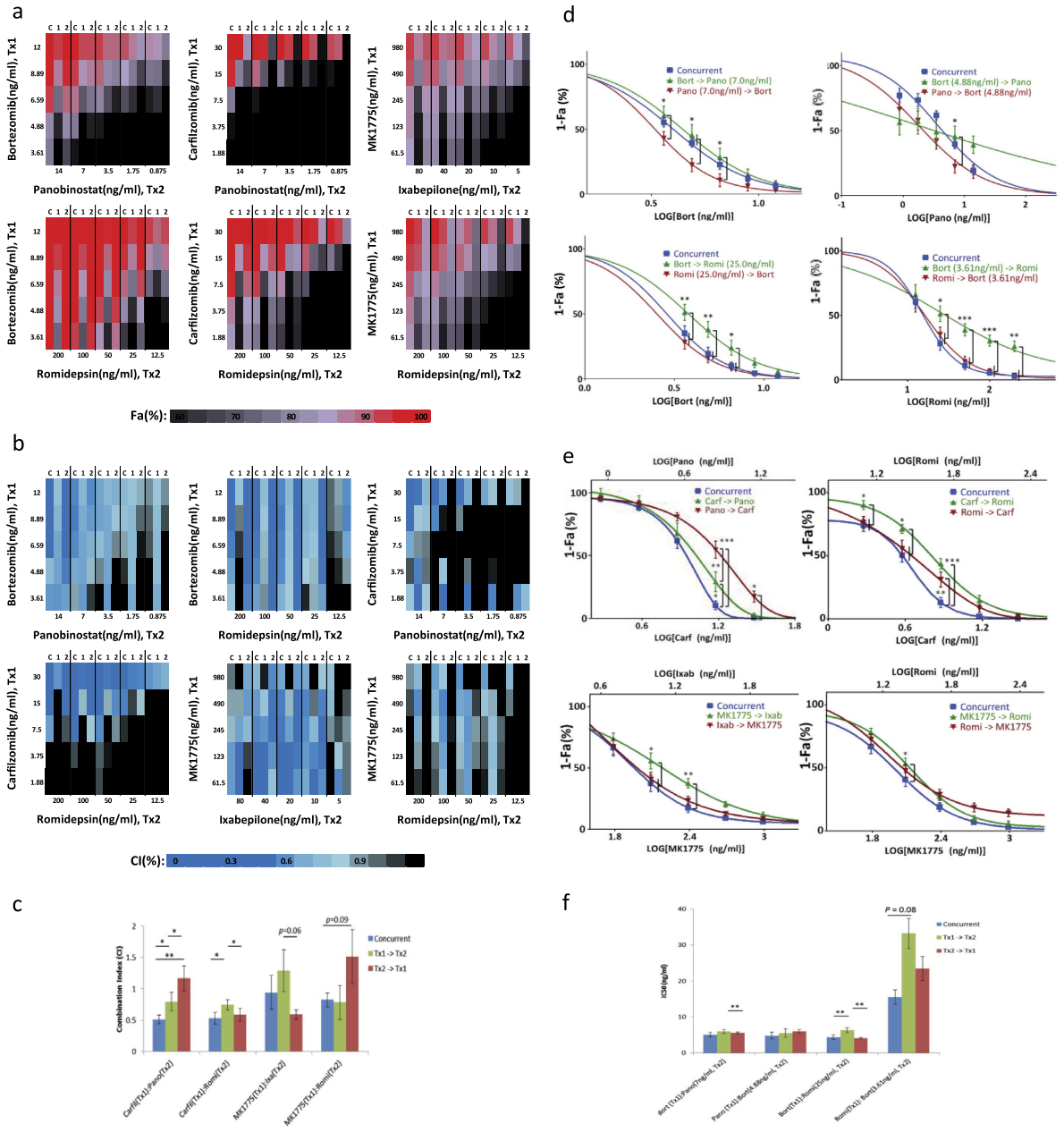

Figure 3. Order-of-addition analysis of the top 6 two-drug combinations assessed in 5 osteosarcoma cell lines FA (a) and CI (b) results using CT-Glo viability assay and non-constant ratio CI method, respectively. *C* indicates concurrent treatment, 1: Tx1 given 24 hours prior to T × 2, 2: T × 2 given 24 hours prior to T × 1. (**c**) combination indices of carfilzomib:romidepsin, carfilzomib:panobinostat, MK1775:romidepsin, MK1775:ixabepilone in panel E averaged across ED80, ED85, ED90, ED95. (**d**) combination drug-response curves of bortezomib:romidepsin (top) and bortezomib:panobinostat (bottom) reported by CT-Glo. (**e**) combination drug-response curves of carfilzomib:romidepsin (3:20), carfilzomib-panobinostat (30:14), MK1775:romidepsin (98:20), MK1775:ixabepilone (98:8) reported by CT-Glo. (**f**) IC50 values of bortezomib:panobinostat and bortezomib:romidepsin combinations in panel A. Statistical comparison used two-way ANOVA with post-hoc Tukey test (**d,e**) and 2-tail paired *t*-test (**c,f**). *$P < 0.05$, **$P < 0.01$, ***$P < 0.001$).

6 (Table 2). Interestingly, although synergistic, reduced efficacy was observed for MK1775 and ixabepilone. This could potentially be due to the reduced levels of MK1775 used compared with the cell line experiments.

To determine the toxicity of our top candidates against similar but non-tumor cell types, we tested the cytotoxicity of the combinations using primary MSCs and MSC-derived osteoblasts to assess the

Select Fa and CI values of top six combinations with order-of-addition.																	
		Conc (ng/ml)			MNNG/HOS		143B		MG63		U-2 OS		Saos2		FA	*CI*	P-value, N = 10 (FA; CI)		
Tx1	Tx2	Tx1	Tx2	Order of Addition	FA	*CI*	FA	*CI*	FA	*CI*	FA	*CI*	FA	*CI*	(mean ± SEM)	(mean ± SEM)	*Con vs. 1→2*	*Con vs. 2→1*	*1→2 vs. 2→1*
Bortezomib	Panobinostat	12	14	*Concurrent*	1.00	*0.43*	1.00	*0.38*	1.00	*0.60*	1.00	*0.12*	0.95	*0.60*	0.99 ± 0.01	*0.44* ± 0.08	0.016; <0.001	0.141; 0.111	0.228; <0.001
				Tx1 → Tx2	0.95	*0.85*	1.00	*0.94*	0.99	*0.88*	0.95	*0.42*	0.78	*0.64*	0.94 ± 0.02	*0.76* ± 0.06			
				Tx2 → Tx1	0.94	*0.54*	1.00	*0.36*	0.96	*0.44*	1.00	*0.07*	0.99	*0.25*	0.98 ± 0.01	*0.34* ± 0.06			
Bortezomib	Romidepsin	12	200	*Concurrent*	1.00	*0.35*	1.00	*0.91*	1.00	*0.59*	1.00	*0.12*	1.00	*0.48*	1.00 ± 0.00	*0.50* ± 0.09	0.010; 0.001	0.040; 0.010	0.026; <0.001
				Tx1 → Tx2	0.97	*0.77*	1.00	*0.82*	0.99	*0.83*	0.98	*0.41*	0.93	*0.99*	0.98 ± 0.01	*0.77* ± 0.07			
				Tx2 → Tx1	0.99	*0.36*	1.00	*0.39*	1.00	*0.11*	1.00	*0.07*	1.00	*0.51*	1.00 ± 0.00	*0.27* ± 0.06			
Carfilzomib	Panobinostat	30	14	*Concurrent*	0.98	*0.33*	1.00	*0.36*	1.00	*0.39*	1.00	*0.05*	1.00	*0.23*	1.00 ± 0.00	*0.28* ± 0.07	0.051; <0.001	0.002; 0.004	0.002; 0.090
				Tx1 → Tx2	0.91	*0.61*	1.00	*0.58*	1.00	*0.62*	0.99	*0.21*	0.98	*0.54*	0.98 ± 0.01	*0.52* ± 0.08			
				Tx2 → Tx1	0.60	*0.78*	0.90	*0.53*	0.81	*1.18*	0.85	*0.75*	1.00	*0.20*	0.83 ± 0.04	*0.73* ± 0.13			
Carfilzomib	Romidepsin	30	200	*Concurrent*	0.99	*0.21*	1.00	*0.49*	1.00	*0.37*	1.00	*0.08*	1.00	*0.60*	1.00 ± 0.00	*0.35* ± 0.07	0.010; 0.003	0.039; 0.459	0.659; 0.022
				Tx1 → Tx2	0.93	*0.61*	1.00	*0.65*	1.00	*0.66*	0.96	*0.53*	0.97	*0.65*	0.97 ± 0.01	*0.62* ± 0.08			
				Tx2 → Tx1	0.91	*0.55*	1.00	*0.50*	1.00	*0.12*	0.98	*0.34*	1.00	*0.31*	0.98 ± 0.01	*0.34* ± 0.08			
MK1775	Ixabepilone	980	80	*Concurrent*	0.96	*0.85*	0.98	*0.49*	0.87	*1.67*	0.93	*0.50*	0.97	*0.96*	0.94 ± 0.01	*0.89* ± 0.17	0.003; 0.446	0.070; 0.113	0.014; 0.054
				Tx1 → Tx2	0.89	*1.29*	0.96	*0.43*	0.82	*1.42*	0.82	*0.99*	0.94	*0.79*	0.88 ± 0.02	*1.02* ± 0.16			
				Tx2 → Tx1	0.93	*0.77*	0.97	*0.36*	0.88	*0.75*	0.86	*0.58*	0.96	*0.98*	0.92 ± 0.01	*0.69* ± 0.12			
MK1775	Romidepsin	980	200	*Concurrent*	0.95	*0.80*	0.97	*1.42*	0.94	*0.64*	0.99	*0.16*	0.99	*1.28*	0.97 ± 0.01	*0.86* ± 0.18	0.144; 0.277	0.007; 0.024	0.303; 0.066
				Tx1 → Tx2	0.87	*1.46*	0.99	*0.23*	0.92	*0.80*	0.94	*0.65*	0.99	*0.46*	0.94 ± 0.02	*0.73* ± 0.22			
				Tx2 → Tx1	0.85	*1.17*	0.79	*3.36*	0.77	*1.53*	0.93	*0.49*	0.99	*1.58*	0.86 ± 0.03	*1.62* ± 0.41			

Table 1. Select Fa and CI values of top six combinations with order-of-addition.

Ex vivo synergy analysis of top 6 drug combinations								
		Panobinostat (ng/ml)				Romidepsin (ng/ml)			
		8		20		80		200	
		Fa (%)	*CI*	Fa (%)	*CI*	Fa (%)	*CI*	Fa (%)	*CI*
Bortezomib (ng/ml)	4.8	98.5 ± 0.6	*0.48*	97.8 ± 0.1	*0.68*	96.4 ± 1.9	*0.41*	96.7 ± 0.7	*0.71*
	12	97.9 ± 0.1	*0.38*	96.1 ± 0.1	*0.58*	97.9 ± 0.1	*0.60*	97.4 ± 0.5	*1.43*
Carfilzomib (ng/ml)	12	98.2 ± 0.7	*0.35*	98.5 ± 0.1	*0.79*	98.5 ± 0.2	*0.81*	98.3 ± 0.1	*0.62*
	30	97.4 ± 0.3	*0.26*	97.4 ± 0.1	*0.64*	98.1 ± 0.2	*0.29*	95.2 ± 2.1	*0.52*
		Ixabepilone (ng/ml)				Romidepsin (ng/ml)			
		30		75		80		200	
		Fa (%)	*CI*	Fa (%)	*CI*	Fa (%)	*CI*	Fa (%)	*CI*
MK1775 (ng/ml)	200	31.9 ± 2.7	*0.14*	37.3 ± 6.0	*0.17*	98.9 ± 0.1	*0.29*	98.5 ± 0.3	*0.46*
	500	29.6 ± 5.0	*0.19*	31.4 ± 1.3	*0.32*	98.5 ± 0.1	*0.12*	97.8 ± 0.1	*0.31*

Table 2. *Ex vivo* synergy analysis of top 6 drug combinations at clinically achievable concentrations using xenograft model.

sensitivity of non-cancer cells to our drug combinations. Strikingly, our combinations of interest showed reduced toxicity in primary MSCs and MSC-derived osteoblasts compared to the osteosarcoma cells (Fig. 4). Furthermore, the MSC-derived osteoblasts appeared to have higher tolerance than the MSCs, suggesting that the drug combinations may preferentially affect proliferating cells over quiescent cell populations

Discussion

In this study, we tested 54 clinically utilized agents with varied mechanisms of action to better prioritize these agents for potential clinical trials or additional preclinical testing in osteosarcoma. This was done

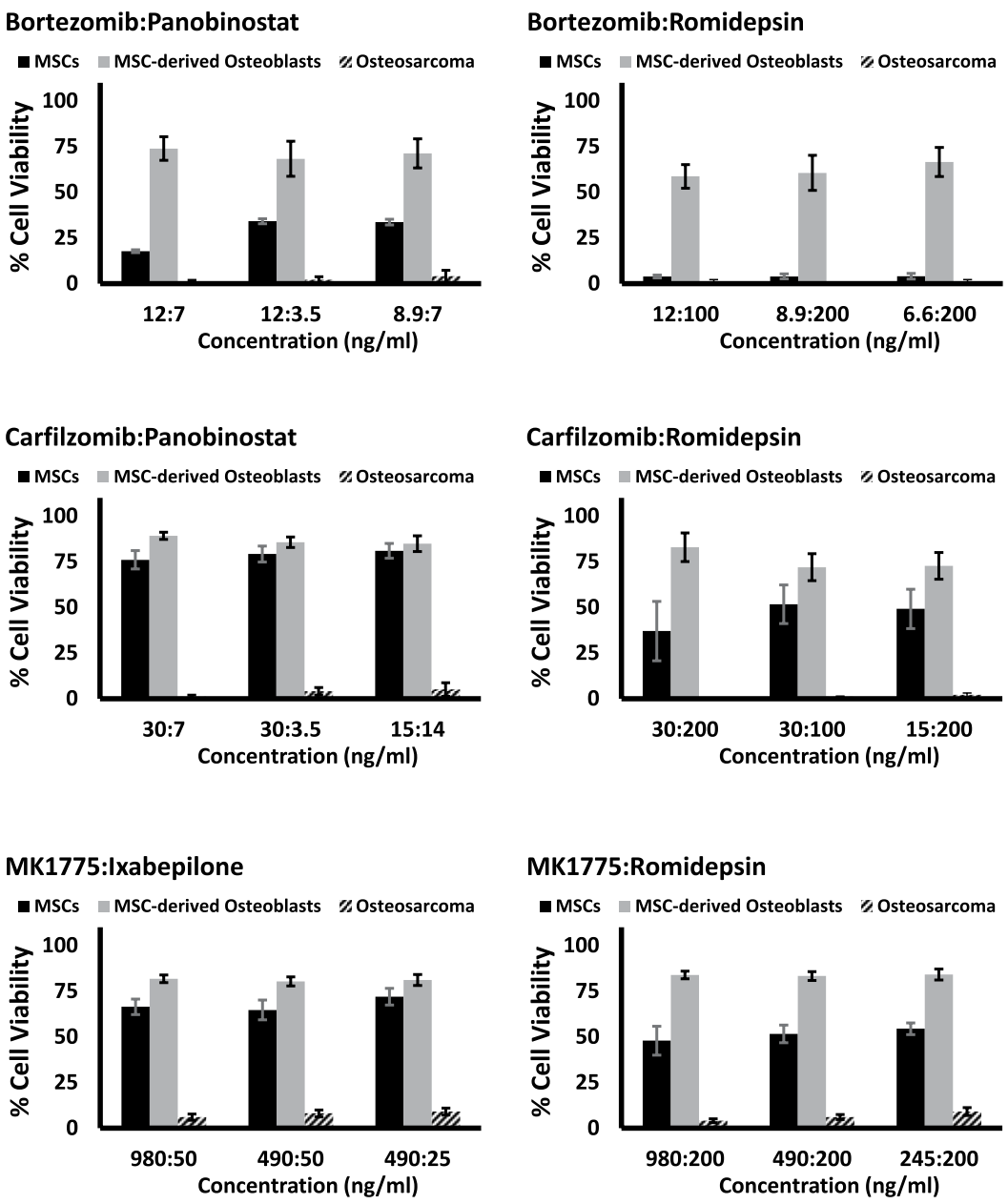

Figure 4. Cytotoxicity of top 6 combinations evaluated in primary MSCs and primary MSC-derived osteoblasts in comparison with osteosarcoma cell lines.

in a relatively high-throughput fashion to determine synergistic combinations of chemotherapies for osteosarcoma, and we report multiple 2-drug combinations with impressive *in vitro* activity. We also tested combinations of targeted agents and found multiple combinations that demonstrated synergy in our tested cell line models. We consistently observed that HDAC and proteasome inhibitor combinations demonstrated good activity. The Wee1 inhibitor MK1775 was also particularly active with romidepsin or ixabepilone.

Both HDAC and proteasome inhibitors have mechanisms of action that result in multiple effects on cellular processes[28–31]. Both have been implicated in cell cycle disruption and lead to apoptosis in multiple models[28,29,32,33]. The antitumor effects of HDAC inhibitors may be related to epigenetic effects on DNA and resultant transcriptional modification of many genes including perhaps a common gene set in malignant cells[32]. HDACs have numerous other roles in the cell, perhaps through epigenetic modification but also through an increasingly clear effect on many other proteins that are modified or interact with HDACs[29,31]. These include roles in cell cycle, reactive oxygen species production, apoptosis, immunomodulatory effects, angiogenesis, and tumor metastasis[29]. Our tested HDAC inhibitors have broad spectrum activity, inhibiting class I and II HDACs (panobinostat and vorinostat), although romidepsin demonstrates some selectivity toward class I HDACs 1 and 2[29,31].

Investigations of HDAC inhibitors in canine osteosarcoma cells have proposed perturbations in the oxidative phosphorylation, cytoskeleton remodeling, cell cycle, and ubiquitin-proteasome pathways by gene expression analysis[34]. Another investigation of a drug-resistant cell line treated with both an HDAC and a DNA methyltransferase inhibitor pointed to apoptosis and differentiation pathways as key mechanisms of action[35]. Others have proposed a miRNA mechanism through c-MYC, again requiring DNA methytransferase inhibitors for an effect[36]. The HDAC inhibitor valproic acid, not active by our methods, has sensitized canine osteosarcoma to doxorubicin[34].

The proteasome inhibitors that we investigated, bortezomib and carfilzomib, have a clearer target of action, namely the 20S subunit of the 26S proteasome, than the HDAC inhibitors, which inhibit a process involving a plethora of different cellular proteins. The effects of inhibiting the proteasome are many, however, with aggregation of numerous proteins from a multitude of pathways usually resulting in cellular dysfunction and often leading to apoptosis. Some of these cellular processes include angiogenesis, the cell cycle, the unfolded protein response, metastasis, and tumor-stromal interactions[28,37]. Intriguingly, one study has shown that proteasome inhibition with bortezomib leads to osteoblast differentiation and increased bone formation[38]. This has also been observed clinically, where bortezomib activity is associated with osteoblast activation, especially in myeloma patients who have a rapid response[39]. Others have explored proteasome inhibitors in osteosarcoma and have proposed as potential mechanisms increased MAPK pathway activity and apoptosis[40], decreased invasion and increased G2M cell cycle arrest[41], and increased apopotosis through RUNX2 stabilization[42]. Pathologically, osteosarcomas are characterized by observable osteoid production. Osteoid is largely composed of type I collagen, a highly expressed protein in osteosarcomas[43]. This focus on protein production and continual endoplasmic reticular stress may underlie osteosarcoma sensitivity to proteasome inhibition (personal communication, Paul Meltzer).

Because it has been suggested that HDAC inhibitors inhibit the proteasome pathway[34] and proteasome inhibition decreases HDAC inhibitor levels[44], this combination has a biologic rationale for synergy[37]. This combination has also been clinically studied in multiple myeloma, along with dexamethasone, with good tolerability and effect at doses and a schedule similar to single-agent use[45]. The most commonly observed side effects were hematologic, including thrombocytopenia, along with neuropathic effects and fatigue. Panobinostat has recently received FDA approval for this indication following a trial with panobinostat and bortezomib in patients with multiple myeloma (NCT01023308). A completed study with bortezomib and vorinostat has demonstrated safety in the pediatric population, with toxicities similar to adult studies (i.e., predominantly neuropathic and hematologic)[46]. A single osteosarcoma patient was treated on this trial without a response.

The Wee1 inhibitor MK1775 has been demonstrated to have effects on sarcomas, including osteosarcoma[12,13,15]. While inhibition of Wee1 initially seemed straightforward mechanistically, it has become more apparent that this protein's function includes coordination of the cell cycle via modification of histones, along with replication fork transcription initiation during S phase[47,48]. Thus, HDAC and proteasome inhibitors and the MK1775 inhibitor share cell cycle disruption as a mechanism, perhaps suggesting that osteosarcoma is remarkably vulnerable to this particular perturbation. In combination, the synergism of MK1775 and romidepsin may stem from manipulation of the cell cycle at the G2/M checkpoint by MK1775, thereby enhancing the lethality of romidepsin possibly through preventing DNA repair mechanisms[49].

We observed a range of activity among the microtubule agents, which either stabilized or inhibited polymerization of beta-tubulin during mitosis. Among members of this class of drugs, which have consistently demonstrated some effectiveness in the Pediatric Preclinical Testing Program, we determined that ixabepilone had the best activity across cell lines[11,50,51]. A phase II study of ixabepilone based on murine xenograft work included 11 osteosarcoma patients without any responses and only a single patient receiving more than 2 cycles of therapy[52,53]. Relatedly, the phase II study for eribulin (NCT02097238), another modulator of microtubule dynamics, which is currently enrolling patients, will help determine if the xenograft preclinical system signal translates into some clinical activity. Because MK1775 abrogates the G2/M checkpoint by inhibiting Wee1, there is a clear rationale for a microtubule inhibitor to have increased activity with forced mitotic entry. Interestingly, the MK1775-ixabepilone combination was the only one with substantially different activity when studied in our *ex vivo* assay, perhaps suggesting a protective effect of the microenvironment.

We have attempted at all phases of our methodology to recapitulate human pharmacokinetics in our testing in terms of concentrations, duration, and protein binding. We recognize that for some agents serum levels may over-represent agent delivery to tumor cells and in other situations it may underestimate conditions in the tumor and its microenvironment. Unfortunately, intratumoral concentrations of many agents are not available. We also recognize that not all agent effects can be determined *in vitro* and that we may have dismissed agents with eventual clinical activity. Among tyrosine kinase inhibitors, the most common class of FDA-approved agents and the most common mechanism among our tested agents, we measured little activity. This could be because these agents have anti-angiogenic or stromal effects clinically, which we could not measure *in vitro* or because of clinically targeted kinases not playing a significant role in osteosarcoma tumor cell biology. Sorafenib has promising osteosarcoma activity clinically that is worthy of further exploration but was not very active in our system, for example[54,55]. Others have demonstrated better activity of kinase inhibitors *in vivo* than *in vitro* in a neuroblastoma preclinical study, which may be due to effects on angiogenesis or other stromal effects[56]. Nonconjugated

immunotherapies or agents with stromal or other non-tumor targets would similarly not be predicted to have any detectable activity in our system as well. Importantly, we acknowledge that this system is intended to explore a number of agents and combinations that could not reasonably be investigated in patients or animal models due to the sheer number of untested agents in osteosarcoma. It is yet to be proven that the methods of incorporating clinically achievable concentrations and modulating levels based on the half-life of agents will be more informative for clinical translation than prior *in vitro* studies that haven't incorporated human pharmacokinetic data.

The methods presented here demonstrate a comprehensive, reproducible, and high-throughput method for exploring antitumor effects of combinations of therapies. In particular, we discovered that combinations of proteasome and HDAC inhibitors demonstrate excellent activity against osteosarcoma cell lines. The 4 most active agents in these classes are all FDA-approved for other indications, which may help with availability for further study. Additionally, MK1775 with ixabepilone would be interesting for early-phase clinical trials.

Combinations of targeted, targeted and cytotoxic, or multiple cytotoxic agents can be explored with this methodology. Particularly for diseases such as osteosarcoma that have few presently available treatments avenues, this important early preclinical data can serve as the basis for confirmatory assays, explorations into the mechanisms of the most promising agents, canine or xenograft studies, and ultimately clinical trials.

Methods

Ethics Statement. All patient samples were obtained in accordance with the guidelines mandated by the Total Cancer Care Protocol as approved by the Institutional Review Board at Moffitt Cancer Center. All patients provided written informed consent prospectively. All procedures involving animals were approved by and carried out in accordance with the guidelines mandated by the Moffitt Cancer Center Institutional Animal Care and Use Committee.

Investigational agents. Agents used included both cytotoxic and targeted agents (most obtained directly from SelleckChem, Sequoia, and Sigma-Aldrich; Supplemental Table S1). Stock solutions were made for each compound in DMSO at 4000× concentrations used in experiments. Structures for all agents are publicly available.

Cell culture. Osteosarcoma cell lines were obtained from ATCC (Manassas, VA). Cells were maintained in DMEM with 15% FBS according to manufacturer's recommendations. Cells were grown at 37 °C and 5% CO_2. All cell lines tested free of mycoplasma every 3 months with MycoAlert tests (Lonza Rockland, Rockland, ME). Cell line identity was confirmed using StemElite ID system (Promega, Madison, WI) using the manufacturer's instructions and the ATCC STR profile database.

Single-agent screening. Single-agent activities of a panel of 54 therapeutic candidates (Supplemental Table S1) were characterized with 5 pediatric osteosarcoma cell lines (143B, MNNG/HOS, MG63, U2OS, Saos2). Human pharmacokinetic data were collected for all agents from previously reported phase I studies, using pediatric and combination studies when available (Supplemental Table S1). For agents with half-lives <8 hours and dosing schedule that was not continuous, agents were applied to the cell lines for 6 hours then removed by 1:125 medium dilution. The remaining agents with longer half-lives were applied for 72 hours. Single-agent anti-tumor activities were assessed at the maximum concentration (C_{max}), 20% C_{max}, and 4% C_{max} using Caspase-Glo and CellTiter-Glo luminescence assays at 24 and 72 hours.

Two-drug combination screening. A 5×5 checker-board matrix format was used to assess all two-drug combinations at five clinically achievable concentrations. Each combination was evaluated at multiple drug ratios to identify synergy (Supplemental Figure S1A). In cases where the same dilution factors were used for both drugs of the combination, diagonals of the 5×5 checker-board matrix provide the effects of the drug combination at constant drug ratio. Full dose-response curves were obtained for each individual drug, and the combination index (CI) for all combinations were calculated using CalcuSyn 2.0 and custom-designed analysis package based on the Chou-Talalay method (Supplemental Figure S1C).

Cell viability assays. The activity levels of single agents and combinations were determined by a high-throughput CellTiter-Glo cell viability assay (Promega). Cells ($1–2 \times 10^3$) were plated in each well of 384–well plates using a Precision XS liquid handling station (Bio-Tek Instruments, Winooski, VT) and incubated overnight. Drug source plates were prepared in 96-well Megatiter plates (Neptune Scientific, San Diego, CA), and the Precision XS station was used to transfer drugs to four replicate wells with an additional four control wells receiving DMSO vehicle control without drug. At the end of the drug incubation period, CellTiter-Glo or Caspase-Glo reagent was added to each well at 1:1 ratio (v/v) with media. The luminescence of the product of viable cells was measured with a Synergy 4 microplate reader (Bio-Tek Instruments). The luminescence data were transferred to Microsoft Excel to calculate percent viability. IC50 values were determined using a sigmoidal equilibrium model regression and XLfit version

5.2 (ID Business Solutions). The IC50 values obtained from single-drug cell viability assays were used to design subsequent drug combination experiments. High-throughput two-agent combination screening experiments were performed using a 5×5 matrix format in 384-well plates to interrogate 25 individual concentration ratios per combination (Supplemental Figure S1).

Analysis of additive and synergistic effects in combination screening data. For drug combination experiments, the CellTiter-Glo assay was used to measure cell viability, with results analyzed for synergistic, additive, or antagonistic effects using primarily the CI method of Chou-Talalay[57] with additional supporting analysis from Fold of Potentiation (FOP) and the MixLow method developed by Boik and colleagues[58]. For the CI method, the dose-effect curve for each drug was determined based on experimental observations using the median-effect principle and was compared to the effect achieved with the 2-drug combination to derive a CI value. This method involves plotting dose-effect curves for each single agent using the median-effect equation: fa/fu = (D/Dm)m, where D = dose of the drug, Dm = dose required for 50% effect, fa and fu = affected and unaffected fractions, respectively (fa = 1−fu), and m = exponent signifying the sigmoidicity of the dose-effect curve. XLfit computer software was used to calculate Dm and m. CIs used for the analysis of the drug combinations were determined by the isobologram equation for mutually nonexclusive drugs that have different modes of action: $CI = (D)_1/(Dx)_1 + (D)_2/(Dx)_2 + (D)_1(D)_2/(Dx)_1(Dx)_2$, where $(Dx)_1$ and $(Dx)_2$ in the denominators are the doses (or concentrations) for D_1 (Drug1) and D_2 (Drug2) alone that gives x% inhibition, whereas $(D)_1$ and $(D)_2$ in the numerators are the doses of Drug1 and Drug2 in combination that also inhibited x% (i.e., isoeffective). CI calculations were done in custom Microsoft Excel templates and verified with CalcuSyn 2.0 (Biosoft, Cambridge, UK). $CI < 1$, $CI = 1$, and $CI > 1$ indicate synergism, additive effects, and antagonism, respectively.

FOP and Mixlow methods were used to further confirm CI synergy calculations. FOP was used for combination screening data with non-constant molar ratios to demonstrate the enhancement of one drug's effect by another by measuring shift in IC50[25,59]. Curve fitting for FOP was performed using Prism V6.05 (GraphPad Software, La Jolla, CA, www.graphpad.com). Dose-response plots for single agents and drug combinations were fitted using a four-parameter non-linear least-squares regression model. Curves were extrapolated to relevant maximum and minimum response levels. The Mixlow method uses a non-linear mixed-effects model in combination with simulations of a sham mixture of a drug with itself to provide confidence intervals for the Loewe interaction index. Loewe interaction indices $LI < 1$, $LI = 1$, and $LI > 1$ indicate synergism, additive effects, and antagonism, respectively. Mixlow calculations were done using Mixlow package 1.0[59].

Cluster analysis. Prior to clustering, fraction affected (FA) and CI data were log-transformed and normalized to a common scale by multiplying the log-transformed 1-FA by a coefficient of 1/3. To provide values suitable for inputting into subsequent cluster analysis, both variables were multiplied by −10. Cluster analysis was accomplished with the use of Cluster 3.0 (Stanford University Labs, Stanford, CA). Complete-linkage unsupervised hierarchical clustering of FA and CI values together was performed using uncentered absolute correlation similarity metrics. Java TreeView 1.1.6r4 (Stanford University Labs) was employed to visualize clustered data.

Apoptosis assay. Caspase-3/7 activation was measured using a 384-well plate based Caspase-Glo 3/7 (Promega) luminescent assay. Cells were treated for 24 hours with serial dilutions of each compound and assessed with Caspase-Glo reagent at 1:1 ratio with media. Luminescence was measured with a Synergy 4 microplate reader (Bio-Tek Instruments).

Tumor xenograft development. Fresh cancer tissues, obtained from surgical specimens of patients undergoing resection for osteosarcoma at the Moffitt Cancer Center, were established as subcutaneous xenografts in female athymic (nu+/nu+) mice (Harlan Laboratories, Washington, DC) (F1 generation). The tumor xenografts from the F1 generation were harvested and reimplanted subcutaneously in groups of five mice for each patient (F2 generation). Tumors were allowed to grow to 1.5 cm, at which point they were harvested, divided into ~3-mm^3 pieces, and transplanted to another 18–22 mice (F3 generation). Tumors from the F3 generation were grown until reaching ~200 mm^3 before harvesting for ex vivo assays.

***Ex vivo* assay.** Tumor cells were collected by fine-needle aspiration from the xenograft animals using a sterile 25G short needle. After tumor samples were microscopically confirmed to be enriched for cancer cells, they were immediately transferred into 10 mL sterile prewarmed complete RPMI 1640 culture medium containing 10% FBS, penicillin (200 μg/mL), and streptomycin (200 μg/mL). Cells were stained with trypan blue and suspended in PBS to assess viability. The viable (membrane intact) and dead cells were then counted, and the total viable cell count was used to calculate final working cell concentrations. ~10,000 viable tumor cells were seeded into each well of a 96-well polystyrene microplate. Cells were treated in duplicate with DMSO (vehicle control) or the top six compounds as single agents and 2-drug combinations in a humidified 5% CO_2 incubator at 37 °C for 72 hours. Cell viability was assessed using CellTiter-Glo.

Isolation, culture, and osteogenic differentiation of murine mesenchymal stem cells. Isolation and culture of mesenchymal stem cells (MSCs) were adopted from published protocol[60]. Hind legs were collected from 6 non-tumor-bearing 4–6 week-old C57/BL6 Rag2−/− mice and placed in sterile PBS. Excess tissue was removed and bones were rinsed in 75% ethanol and dried. Ends were trimmed and bone marrow was flushed three times with sterile PBS to deplete the hematopoietic cells. Bones were cut into 1–3 mm chips, digested with 1 mg/mL collagenase II (Invitrogen, Carlsbad, CA) in α-MEM with 15% FBS, and shaken 1 hour in 37 °C at 150 RPM. Digested bone fragments were grown in 6-well tissue culture plates in α-MEM with 15% FBS. Medium was changed every 3 days. For osteogenic differentiation, MSCs were seeded at 6,000 cells/well in 48-well plates and cultured until 100% confluent. 20× StemXVivo mouse/rat osteogenic supplement (R&D Systems, #CCM009) was added to media and changed every 2–3 days for 14–21 days Cells were washed with PBS, fixed in 10% buffered formalin for 15 minutes, rinsed twice with ddH_2O, and then stained for 45 minutes in the dark using 4% alizarin red (Fisher Scientific, #AC400480250) to verify osteogenic differentiation. pH was adjusted to 4.2 using 10% NH_4OH. After stain was removed, cells were washed 4 times with ddH_2O and allowed to dry. Bright red stain showing calcium deposits was confirmed visually.

References

1. Bielack, S. *et al.* MAP plus maintenance pegylated interferon α-2b (MAPIfn) versus MAP alone in patients with resectable high-grade osteosarcoma and good histologic response to preoperative MAP: First results of the EURAMOS-1 "good response" randomization. *Journal of Clinical Oncology*, *2013 ASCO Annual Meeting Abstracts.* **31** (2013).
2. Ebb, D. *et al.* Phase II trial of trastuzumab in combination with cytotoxic chemotherapy for treatment of metastatic osteosarcoma with human epidermal growth factor receptor 2 overexpression: a report from the children's oncology group. *J Clin Oncol* **30,** 2545–2551, doi: 10.1200/JCO.2011.37.4546 (2012).
3. Goldsby, R. E. *et al.* Feasibility and dose discovery analysis of zoledronic acid with concurrent chemotherapy in the treatment of newly diagnosed metastatic osteosarcoma: a report from the Children's Oncology Group. *European journal of cancer* **49,** 2384–2391, doi: 10.1016/j.ejca.2013.03.018 (2013).
4. Meyers, P. A. *et al.* Osteosarcoma: a randomized, prospective trial of the addition of ifosfamide and/or muramyl tripeptide to cisplatin, doxorubicin, and high-dose methotrexate. *J Clin Oncol* **23,** 2004–2011, doi: 10.1200/jco.2005.06.031 (2005).
5. Meyers, P. A. *et al.* Osteosarcoma: the addition of muramyl tripeptide to chemotherapy improves overall survival—a report from the Children's Oncology Group. *J Clin Oncol* **26,** 633–638, doi: 10.1200/JCO.2008.14.0095 (2008).
6. Collins, M. *et al.* Benefits and adverse events in younger versus older patients receiving neoadjuvant chemotherapy for osteosarcoma: findings from a meta-analysis. *Journal of clinical oncology : official journal of the American Society of Clinical Oncology* **31,** 2303–2312, doi: 10.1200/JCO.2012.43.8598 (2013).
7. Haddox, C. L. *et al.* Osteosarcoma in pediatric patients and young adults: a single institution retrospective review of presentation, therapy, and outcome. *Sarcoma* **2014,** 402509, doi: 10.1155/2014/402509 (2014).
8. Janeway, K. A. *et al.* Outcome for adolescent and young adult patients with osteosarcoma: a report from the Children's Oncology Group. *Cancer* **118,** 4597–4605, doi: 10.1002/cncr.27414 (2012).
9. Biermann, J. S. *et al.* Bone cancer. *J Natl Compr Canc Netw* **11,** 688–723 (2013).
10. Administration, U. S. F. A. D. "Hematology/Oncology (Cancer) Approvals & Safety Notifications",<http://www.fda.gov/drugs/informationondrugs/approveddrugs/ucm279174.htm> (2013) (Date of access:01/04/2015).
11. Sampson, V. B., Gorlick, R., Kamara, D. & Anders Kolb, E. A review of targeted therapies evaluated by the pediatric preclinical testing program for osteosarcoma. *Frontiers in oncology* **3,** 132, doi: 10.3389/fonc.2013.00132 (2013).
12. Kreahling, J. M. *et al.* Wee1 inhibition by MK-1775 leads to tumor inhibition and enhances efficacy of gemcitabine in human sarcomas. *PLoS One* **8,** e57523, doi: 10.1371/journal.pone.0057523 (2013).
13. Kreahling, J. M. *et al.* MK1775, a selective Wee1 inhibitor, shows single-agent antitumor activity against sarcoma cells. *Molecular cancer therapeutics* **11,** 174–182, doi: 10.1158/1535-7163.MCT-11-0529 (2012).
14. Fu, W. *et al.* The Cyclin-Dependent Kinase Inhibitor SCH 727965 (Dinaciclib) Induces the Apoptosis of Osteosarcoma Cells. *Molecular cancer therapeutics* **10,** 1018–1027, doi: 10.1158/1535-7163.MCT-11-0167 (2011).
15. Fu, W. *et al.* Apoptosis of osteosarcoma cultures by the combination of the cyclin-dependent kinase inhibitor SCH727965 and a heat shock protein 90 inhibitor. *Cell death & disease* **4,** e566, doi: 10.1038/cddis.2013.101 (2013).
16. Withrow, S. J. & Khanna, C. Bridging the gap between experimental animals and humans in osteosarcoma. *Cancer treatment and research* **152,** 439–446, doi: 10.1007/978-1-4419-0284-9_24 (2009).
17. Parashar, S. *et al.* S-adenosylmethionine blocks osteosarcoma cells proliferation and invasion *in vitro* and tumor metastasis *in vivo*: therapeutic and diagnostic clinical applications. *Cancer Med* **4,** 732–744, doi: 10.1002/cam4.386 (2015).
18. Fan, T. M. Animal models of osteosarcoma. *Expert Rev Anticancer Ther* **10,** 1327–1338, doi: 10.1586/era.10.107 (2010).
19. Gorlick, R., Janeway, K., Lessnick, S., Randall, R. L. & Marina, N. Children's Oncology Group's 2013 blueprint for research: Bone tumors. *Pediatric blood & cancer* **60,** 1009–1015, doi: 10.1002/pbc.24429 (2013).
20. Weiss, A. *et al.* Advances in therapy for pediatric sarcomas. *Curr Oncol Rep* **16,** 395, doi: 10.1007/s11912-014-0395-z (2014).
21. Chen, X. *et al.* Recurrent somatic structural variations contribute to tumorigenesis in pediatric osteosarcoma. *Cell reports* **7,** 104–112, doi: 10.1016/j.celrep.2014.03.003 (2014).
22. Chandar, N., Billig, B., McMaster, J. & Novak, J. Inactivation of p53 gene in human and murine osteosarcoma cells. *Br J Cancer* **65,** 208–214 (1992).
23. Romano, J. W. *et al.* Identification and characterization of a p53 gene mutation in a human osteosarcoma cell line. *Oncogene* **4,** 1483–1488 (1989).
24. Florenes, V. A. *et al.* MDM2 gene amplification and transcript levels in human sarcomas: relationship to TP53 gene status. *J Natl Cancer Inst* **86,** 1297–1302 (1994).
25. Cubitt, C. L. *et al.* Rapid screening of novel agents for combination therapy in sarcomas. *Sarcoma* **2013,** 365723, doi: 10.1155/2013/365723 (2013).
26. Smith, M. A. & Houghton, P. A proposal regarding reporting of *in vitro* testing results. *Clinical cancer research: an official journal of the American Association for Cancer Research* **19,** 2828–2833, doi: 10.1158/1078-0432.CCR-13-0043 (2013).
27. Janeway, K. A., Place, A. E., Kieran, M. W. & Harris, M. H. Future of Clinical Genomics in Pediatric Oncology. *Journal of clinical oncology: official journal of the American Society of Clinical Oncology*, doi: 10.1200/JCO.2012.46.8470 (2013).
28. Kisselev, A. F., van der Linden, W. A. & Overkleeft, H. S. Proteasome inhibitors: an expanding army attacking a unique target. *Chem Biol* **19,** 99–115, doi: 10.1016/j.chembiol.2012.01.003 (2012).

29. Bolden, J. E., Peart, M. J. & Johnstone, R. W. Anticancer activities of histone deacetylase inhibitors. *Nat Rev Drug Discov* **5,** 769–784, doi: 10.1038/nrd2133 (2006).
30. Dokmanovic, M., Clarke, C. & Marks, P. A. Histone deacetylase inhibitors: overview and perspectives. *Mol Cancer Res* **5,** 981–989, doi: 10.1158/1541-7786.mcr-07-0324 (2007).
31. Zhang, L. *et al.* Trend of histone deacetylase inhibitors in cancer therapy: isoform selectivity or multitargeted strategy. *Med Res Rev* **35,** 63–84, doi: 10.1002/med.21320 (2015).
32. Bolden, J. E. *et al.* HDAC inhibitors induce tumor-cell-selective pro-apoptotic transcriptional responses. *Cell Death Dis* **4,** e519, doi: 10.1038/cddis.2013.9 (2013).
33. Newbold, A. *et al.* Molecular and biologic analysis of histone deacetylase inhibitors with diverse specificities. *Mol Cancer Ther* **12,** 2709–2721, doi: 10.1158/1535-7163.mct-13-0626 (2013).
34. Wittenburg, L. A., Ptitsyn, A. A. & Thamm, D. H. A systems biology approach to identify molecular pathways altered by HDAC inhibition in osteosarcoma. *J Cell Biochem* **113,** 773–783, doi: 10.1002/jcb.23403 (2012).
35. Capobianco, E. *et al.* Separate and combined effects of DNMT and HDAC inhibitors in treating human multi-drug resistant osteosarcoma HosDXR150 cell line. *PLoS One* **9,** e95596, doi: 10.1371/journal.pone.0095596 (2014).
36. Thayanithy, V. *et al.* Combinatorial treatment of DNA and chromatin-modifying drugs cause cell death in human and canine osteosarcoma cell lines. *PLoS One* **7,** e43720, doi: 10.1371/journal.pone.0043720 (2012).
37. Hideshima, T., Richardson, P. G. & Anderson, K. C. Mechanism of action of proteasome inhibitors and deacetylase inhibitors and the biological basis of synergy in multiple myeloma. *Mol Cancer Ther* **10,** 2034–2042, doi: 10.1158/1535-7163.mct-11-0433 (2011).
38. Garrett, I. R. *et al.* Selective inhibitors of the osteoblast proteasome stimulate bone formation *in vivo* and *in vitro*. *J Clin Invest* **111,** 1771–1782, doi: 10.1172/JCI16198 (2003).
39. Zangari, M. *et al.* Response to bortezomib is associated to osteoblastic activation in patients with multiple myeloma. *Br J Haematol* **131,** 71–73, doi: 10.1111/j.1365-2141.2005.05733.x (2005).
40. Lou, Z. *et al.* Bortezomib induces apoptosis and autophagy in osteosarcoma cells through mitogen-activated protein kinase pathway *in vitro*. *J Int Med Res* **41,** 1505–1519, doi: 10.1177/0300060513490618 (2013).
41. Li, X. *et al.* Proteasome inhibitor MG132 enhances TRAIL-induced apoptosis and inhibits invasion of human osteosarcoma OS732 cells. *Biochem Biophys Res Commun* **439,** 179–186, doi: 10.1016/j.bbrc.2013.08.066 (2013).
42. Shapovalov, Y., Benavidez, D., Zuch, D. & Eliseev, R. A. Proteasome inhibition with bortezomib suppresses growth and induces apoptosis in osteosarcoma. *Int J Cancer* **127,** 67–76, doi: 10.1002/ijc.25024 (2010).
43. Franceschi, R. T., Romano, P. R. & Park, K. Y. Regulation of type I collagen synthesis by 1,25-dihydroxyvitamin D3 in human osteosarcoma cells. *J Biol Chem* **263,** 18938–18945 (1988).
44. Kikuchi, J. *et al.* Histone deacetylases are critical targets of bortezomib-induced cytotoxicity in multiple myeloma. *Blood* **116,** 406–417, doi: 10.1182/blood-2009-07-235663 (2010).
45. Harrison, S. J. *et al.* A high rate of durable responses with romidepsin, bortezomib, and dexamethasone in relapsed or refractory multiple myeloma. *Blood* **118,** 6274–6283, doi: 10.1182/blood-2011-03-339879 (2011).
46. Muscal, J. A. *et al.* A phase I trial of vorinostat and bortezomib in children with refractory or recurrent solid tumors: a Children's Oncology Group phase I consortium study (ADVL0916). *Pediatr Blood Cancer* **60,** 390–395, doi: 10.1002/pbc.24271 (2013).
47. Dominguez-Kelly, R. *et al.* Wee1 controls genomic stability during replication by regulating the Mus81-Eme1 endonuclease. *J Cell Biol* **194,** 567–579, doi: 10.1083/jcb.201101047 (2011).
48. Mahajan, K., Fang, B., Koomen, J. M. & Mahajan, N. P. H2B Tyr37 phosphorylation suppresses expression of replication-dependent core histone genes. *Nat Struct Mol Biol* **19,** 930–937, doi: 10.1038/nsmb.2356 (2012).
49. Zhou, L. *et al.* A regimen combining the Wee1 inhibitor AZD1775 with HDAC inhibitors targets human acute myeloid leukemia cells harboring various genetic mutations. *Leukemia*, doi: 10.1038/leu.2014.296 (2014).
50. Kolb, E. A. *et al.* Initial testing (stage 1) of eribulin, a novel tubulin binding agent, by the pediatric preclinical testing program. *Pediatric blood & cancer* **60,** 1325–1332, doi: 10.1002/pbc.24517 (2013).
51. Lock, R. B. *et al.* Initial testing of the CENP-E inhibitor GSK923295A by the pediatric preclinical testing program. *Pediatr Blood Cancer* **58,** 916–923, doi: 10.1002/pbc.23176 (2012).
52. Peterson, J. K. *et al. In vivo* evaluation of ixabepilone (BMS247550), a novel epothilone B derivative, against pediatric cancer models. *Clin Cancer Res* **11,** 6950–6958, doi: 10.1158/1078-0432.CCR-05-0740 (2005).
53. Jacobs, S. *et al.* Phase II trial of ixabepilone administered daily for five days in children and young adults with refractory solid tumors: a report from the children's oncology group. *Clin Cancer Res* **16,** 750–754, doi: 10.1158/1078-0432.ccr-09-1906 (2010).
54. Grignani, G. *et al.* A phase II trial of sorafenib in relapsed and unresectable high-grade osteosarcoma after failure of standard multimodal therapy: an Italian Sarcoma Group study. *Annals of oncology : official journal of the European Society for Medical Oncology / ESMO* **23,** 508–516, doi: 10.1093/annonc/mdr151 (2012).
55. Grignani, G. *et al.* Sorafenib and everolimus for patients with unresectable high-grade osteosarcoma progressing after standard treatment: a non-randomised phase 2 clinical trial. *Lancet Oncol* **16,** 98–107, doi: 10.1016/S1470-2045(14)71136-2 (2015).
56. Kumar, S. *et al.* Metronomic oral topotecan with pazopanib is an active antiangiogenic regimen in mouse models of aggressive pediatric solid tumor. *Clinical cancer research : an official journal of the American Association for Cancer Research* **17,** 5656–5667, doi: 10.1158/1078-0432.CCR-11-0078 (2011).
57. Chou, T. C. & Talalay, P. Quantitative analysis of dose-effect relationships: the combined effects of multiple drugs or enzyme inhibitors. *Advances in enzyme regulation* **22,** 27–55 (1984).
58. Boik, J. C., Newman, R. A. & Boik, R. J. Quantifying synergism/antagonism using nonlinear mixed-effects modeling: a simulation study. *Stat Med* **27,** 1040–1061, doi: 10.1002/sim.3005 (2008).
59. mixlow: software for assessing drug synergism/antagonism v. R package version 1.0.1 (2012).
60. Zhu, H. *et al.* A protocol for isolation and culture of mesenchymal stem cells from mouse compact bone. *Nat Protoc* **5,** 550–560, doi: 10.1038/nprot.2009.238 (2010).

Acknowledgements

We thank Laura Hall (Moffitt Molecular Genomics Core) for performing cell line identity and Rasa Hamilton (Moffitt Cancer Center) for editorial review of the manuscript. This study was generously supported by the Pediatric Cancer Foundation (www.fastercure.org) and the V Foundation. This work has been supported in part by the Translational Research Core at the H. Lee Moffitt Cancer Center & Research Institute, an NCI designated Comprehensive Cancer Center (P30-CA076292).

Author Contributions

D.Y., D.S. and D.R. conceived the study. D.Y., E.K., C.C. and D.R. designed the experiments. J.M., J.K., S.A. and C.L. provided essential reagents, protocols, and comments on manuscript drafts. D.Y. and E.K. performed the experiments. D.Y., E.K. and C.C. developed the data analysis templates. D.Y., D.R. and E.K. analyzed and processed the data. J.L. provided statistical analysis. D.Y. and D.R. wrote the manuscript. All authors reviewed and authorized the manuscript.

Additional Information

Supplementary information accompanies this paper at http://www.nature.com/srep

Competing financial interests: The authors declare no competing financial interests.

How to cite this article: Yu, D. *et al.* Identification of Synergistic, Clinically Achievable, Combination Therapies for Osteosarcoma. *Sci. Rep.* **5**, 16991; doi: 10.1038/srep16991 (2015).